Optimizing infrared to near infrared upconversion quantum yield of β-NaYF4:Er3+ in fluoropolymer matrix for photovoltaic devices

Optimizing infrared to near infrared upconversion quantum yield of -NaYF4:Er3+ in fluoropolymer matrix for photovoltaic devices

Aruna Ivaturi, Sean K. W. MacDougall, Rosa Martín-Rodríguez, Marta Quintanilla, Jose Marques-Hueso, Karl W. Krämer, Andries Meijerink, and Bryce S. Richards

Citation: Journal of Applied Physics **114**, 013505 (2013); doi: 10.1063/1.4812578
View online: http://dx.doi.org/10.1063/1.4812578
View Table of Contents: http://scitation.aip.org/content/aip/journal/jap/114/1?ver=pdfcov
Published by the AIP Publishing

Optimizing infrared to near infrared upconversion quantum yield of β-$NaYF_4$:Er^{3+} in fluoropolymer matrix for photovoltaic devices

Aruna Ivaturi,[1,a)] Sean K. W. MacDougall,[1] Rosa Martín-Rodríguez,[2] Marta Quintanilla,[1,b)] Jose Marques-Hueso,[1] Karl W. Krämer,[3] Andries Meijerink,[2] and Bryce S. Richards[1,a)]
[1]*Institute of Photonics and Quantum Sciences, School of Engineering and Physical Sciences, Heriot-Watt University, Edinburgh EH14 4AS, United Kingdom*
[2]*Department of Chemistry, Debye Institute for Nanomaterials Science, Utrecht University, Princetonplein 5, 3584 CC Utrecht, The Netherlands*
[3]*Department of Chemistry and Biochemistry, University of Bern, Freiestrasse 3, CH-3012 Bern, Switzerland*

(Received 12 March 2013; accepted 14 June 2013; published online 3 July 2013)

The present study reports for the first time the optimization of the infrared (1523 nm) to near-infrared (980 nm) upconversion quantum yield (*UC-QY*) of hexagonal trivalent erbium doped sodium yttrium fluoride (β-$NaYF_4$:Er^{3+}) in a perfluorocyclobutane (PFCB) host matrix under monochromatic excitation. Maximum *internal* and *external UC-QYs* of $8.4\% \pm 0.8\%$ and $6.5\% \pm 0.7\%$, respectively, have been achieved for 1523 nm excitation of $970 \pm 43\ Wm^{-2}$ for an optimum Er^{3+} concentration of 25 mol% and a phosphor concentration of 84.9 w/w% in the matrix. These results correspond to normalized *internal* and *external* efficiencies of $0.86 \pm 0.12\ cm^2\ W^{-1}$ and $0.67 \pm 0.10\ cm^2\ W^{-1}$, respectively. These are the highest values ever reported for β-$NaYF_4$:Er^{3+} under monochromatic excitation. The special characteristics of both the UC phosphor β-$NaYF_4$:Er^{3+} and the PFCB matrix give rise to this outstanding property. Detailed power and time dependent luminescence measurements reveal energy transfer upconversion as the dominant UC mechanism. © *2013 AIP Publishing LLC*. [http://dx.doi.org/10.1063/1.4812578]

I. INTRODUCTION

Silicon (Si) cells make up for about 90% of the worldwide solar cell production.[1] The Si semiconductor absorbs only sunlight with energies higher than the bandgap of 1.12 eV, corresponding to wavelengths shorter than 1100 nm. Accordingly, around 20% of the incident solar energy is lost because photons with energy below the bandgap of Si are not absorbed by the device.[2] This discrepancy between the energy distribution of the photons in the solar spectrum and the absorption spectrum of Si limits the efficiency of silicon based single-junction photovoltaic (PV) devices. Upconversion (UC) is a novel and promising approach to reduce these sub band gap transmission losses.[3–9]

UC refers to an anti-Stokes type nonlinear optical emission process in which one higher energy photon is emitted for every two or more absorbed lower energy photons.[10] Since the first experimental demonstration in 1966,[11] this effect has received renewed interest due to its ever expanding application base in, for example, lasing,[12] laser cooling,[13] temperature sensing,[14] biomedical imaging and therapy,[15,16] 3D displays,[17] and, more recently, for broadening the spectral response of PV devices.[4–9] In the context of Si PV devices, the UC of the sub-bandgap photons ($\lambda > 1100$ nm) into above-bandgap photons ($\lambda < 1100$ nm) increases the theoretical efficiency limit of a single-junction Si solar cell from near 30% up to 40% when illuminated under non-concentrated light.[2,3] The UC layer is placed at the rear of the device to capture the transmitted photons and thus it is possible to independently optimize the layer for enhanced device performance. The key figure of merit for the UC layer is the quantum yield of the UC process (*UC-QY*). The *internal UC-QY* [*iUC-QY*] is defined as the ratio of the UC photons emitted to the total number of excitation photons *absorbed*, whereas the *external UC-QY* [*eUC-QY*] is defined as the ratio of the UC photons emitted to the total number of *incident* excitation photons. For fundamental understanding and to determine materials potential as spectral converter in conjunction with a PV device, it is important to measure both the *iUC-QY* and *eUC-QY*.

The UC material is usually available as powder and is hence embedded in a host matrix or binding agent for its application to solar cells. The matrix should ideally have the same refractive index as the UC material to reduce light scattering. Also the absorption of light by the matrix has to be negligible for both the absorption and emission spectral regions of the upconverter.[4,8] Therefore, it is important to measure the *iUC-QY* and *eUC-QY* of the UC material in the desired host matrix. Most studies report only the *eUC-QY* of the UC phosphor powder without the host matrix,[8] or estimate it indirectly by applying the UC material in a binding agent to a solar cell.[4] Uncertainties arise in the former case due to scattering of the incident and emitted light by the UC powder,[8] while in the latter case, different loss mechanisms have to be estimated for the calculation of the *UC-QY*.[4]

Trivalent erbium-doped hexagonal sodium yttrium fluoride (β-$NaYF_4$:Er^{3+}) is one of the promising materials for Si-based UC-PV applications with the highest *UC-QY* in the

[a)]Authors to whom correspondence should be addressed. Electronic addresses: A.Ivaturi@hw.ac.uk and B.S.Richards@hw.ac.uk
[b)]Present address: Centre Énergie Matériaux Télécommunications, 800, De La Gauchetière Ouest, Bureau 6900, Montréal (Québec) H5A 1K6, Canada

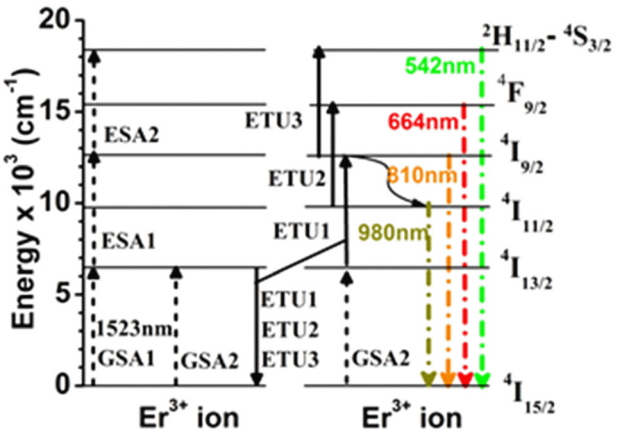

FIG. 1. Energy level diagram of Er^{3+} and UC mechanisms for $^4I_{15/2}$ to $^4I_{13/2}$ excitation. UC emissions are shown as dashed-dotted arrows, GSA/ESA as dashed arrows, and ETU processes as solid arrows. The curved arrows represent fast multi-phonon relaxations.

near infrared (NIR) spectral region.[4,5,8] The Er^{3+} ions have a ladder of nearly equally spaced energy levels [see Figure 1], which are multiples of the $^4I_{15/2} \rightarrow {}^4I_{13/2}$ transition energy.[18] Photons in the 1480 nm to 1580 nm range are absorbed and give rise to four main emission bands: $^4I_{11/2} \rightarrow {}^4I_{15/2}$ at 980 nm, $^4I_{9/2} \rightarrow {}^4I_{15/2}$ at 810 nm, $^4F_{9/2} \rightarrow {}^4I_{15/2}$ at 664 nm, and $^2H_{11/2}$-$^4S_{3/2} \rightarrow {}^4I_{15/2}$ at 542 nm. Due to the low phonon energy of the fluoride host lattice ($\sim$350 cm^{-1}), the multi-phonon relaxation is greatly reduced as compared to oxides ($\sim$600 cm^{-1}) and emissions show high efficiencies.[10] It should be noted that the 980 nm emission accounts for $\sim$97% of the total UC emission in β-$NaYF_4$:Er^{3+} under $^4I_{15/2} \rightarrow {}^4I_{13/2}$ excitation. Additionally, multiple cation sites and microscopic disorder broaden the Er^{3+} absorption spectra in the β-$NaYF_4$ host lattice and thus provides a broader window for harvesting the solar spectrum.[19,20]

Er^{3+} UC emission can be achieved via several mechanisms including ground state absorption (GSA) followed by excited state absorption (ESA) or energy transfer upconversion (ETU), as depicted schematically in Figure 1. GSA/ESA occur when a single Er^{3+} ion is excited to an intermediate excited level from the ground level (GSA1, $^4I_{15/2} \rightarrow {}^4I_{13/2}$) and then a second photon is absorbed within the lifetime of that level populating a higher energy state (ESA1, $^4I_{13/2} \rightarrow {}^4I_{9/2}$). ETU requires two proximate ions, both excited into the intermediate energy state, usually via GSA (GSA1 and GSA2; $^4I_{15/2} \rightarrow {}^4I_{13/2}$). When one ion relaxes to the ground state (down arrow ETU1), rather than by the emission of a photon, the energy is transferred to the neighboring ion raising it into a higher excited state. This is denoted by arrows ETU1, 2, and 3 for the ETU processes. Upon excitation at 1523 nm, Er^{3+} ions in β-$NaYF_4$:Er^{3+} are promoted to the $^4I_{13/2}$ first excited state (GSA1, $^4I_{15/2} \rightarrow {}^4I_{13/2}$). Population of higher Er^{3+} excited states can occur via various processes. An Er^{3+} ion promoted to the $^4I_{9/2}$ excited state via the $^4I_{13/2} \rightarrow {}^4I_{9/2}$ ESA1 and the ($^4I_{13/2}$, $^4I_{13/2}$) $\rightarrow$ ($^4I_{15/2}$, $^4I_{9/2}$) ETU1 processes is responsible for emission around 810 nm. The ($^4I_{13/2}$, $^4I_{13/2}$) $\rightarrow$ ($^4I_{15/2}$, $^4I_{9/2}$) ETU1 process followed by the $^4I_{9/2} \rightarrow {}^4I_{11/2}$ multi-phonon relaxation is responsible for the main $^4I_{11/2}$ UC emission around 980 nm. Additionally, after the population of the $^4I_{11/2}$ Er^{3+} level, the $^4F_{9/2}$ Er^{3+} emitting state is populated via the ($^4I_{11/2}$, $^4I_{13/2}$) $\rightarrow$ ($^4F_{9/2}$, $^4I_{15/2}$) ETU2 process giving rise to red UC emission bands centred at 664 nm. Due to the large energy mismatch ($\sim$1150 cm^{-1}), this process is not very efficient. Also it may be noted that the ($^4I_{13/2}$, $^4I_{13/2}$) $\rightarrow$ ($^4I_{15/2}$, $^4I_{11/2}$) ETU mechanism is not possible due to the large energy mismatch ($\sim$3550 cm^{-1}). For the $^2H_{11/2}$-$^4S_{3/2}$ UC green emission centred at 542 nm, the $^2H_{11/2}$ state is reached by a second ESA2 process within the laser pulse, upon absorption of a 1523 nm photon by an Er^{3+} ion in the $^4I_{9/2}$ excited state. Additionally, ($^4I_{9/2}$, $^4I_{13/2}$) $\rightarrow$ ($^2H_{11/2}$-$^4S_{3/2}$, $^4I_{15/2}$) ETU3 process may contribute to the UC green emission. The most efficient and dominant UC mechanism in β-$NaYF_4$:Er^{3+} is ETU.[4]

The majority of previous studies on UC-PV devices focused on 20 mol% Er^{3+} doped β-$NaYF_4$, which was shown to be the optimum within the limited range of 2, 20, 50, and 100 mol% doped samples under 1523 nm excitation.[4,8] More recently, an extremely high *iUC-QY* of 16.2% $\pm$ 0.5% has been demonstrated in 10 mol% Er^{3+} doped β-$NaYF_4$ when excited by a broadband laser source with bandwidth in the range of 61–80 nm.[21] However, there is a lack of systematic optimization of the Er^{3+} doping in β-$NaYF_4$:Er^{3+} for PV device applications in literature.

In the present study, the *iUC-QY* and *eUC-QY* of β-$NaYF_4$: Er^{3+} have been optimized for 1523 nm (IR) monochromatic excitation and 980 nm (NIR) emission with respect to both the Er^{3+} doping in β-$NaYF_4$ and the β-$NaYF_4$:Er^{3+} phosphor concentration in the perfluorocyclobutane (PFCB) host matrix. PFCB is a semifluorinated polymer of 1,1,1-tris (4-trifluorovinyloxy phenyl) ethane [Tetramer technologies LLC, USA], which cyclopolymerizes on heating.[22] The refractive index of β-$NaYF_4$:20%Er^{3+} was reported as 1.52 and 1.48,[4,23] the absorption coefficients are $\sim$5 cm^{-1} at 1523 nm and $\sim$3 cm^{-1} at 980 nm.[8] PFCB matches the refractive index of β-$NaYF_4$ exhibits a lower absorption than the latter in the region of interest, and thus seems to be a good host matrix for the chosen UC material.[22,24] Moreover, PFCB has no molecular vibrations in the spectral window around 1550 nm where hydrocarbon based polymers typically show strong C-H absorptions.[24,25]

II. EXPERIMENTAL

A. Sample preparation

In the present study, the Er^{3+}doping in the β-$NaYF_4$ host lattice and the concentration of the phosphor (β-$NaYF_4$:Er^{3+}) in the PFCB matrix were optimized for a maximum *UC-QY* of the 980 nm emission upon 1523 nm monochromatic excitation. Samples of the pure hexagonal β-phase with about 10 μm grain size were synthesized according to Ref. 26. β-$NaYF_4$: Er^{3+} samples with Er^{3+} doping of 5%, 10%, 15%, 20%, 25%, 30%, 35%, 40%, 50%, and 75% were prepared. The phosphor powders were embedded in a PFCB matrix with different concentrations from 55.6 to 84.9 w/w% and cured at 160 °C for 18 h. For higher concentrations than 84.9 w/w%, the PFCB could not bind the amount of phosphor anymore. The samples were finally polished to circular pellets of 1 mm thickness and 12.5 mm diameter.

B. Sample characterizations

Monochromatic excitation light was selected from a supercontinuum laser (Fianium SC400 6 W) with a double monochromator. The absorbance, upconversion emission, excitation, *iUC-QY*, and *eUC-QY* of the samples were measured using a calibrated spectrofluorometer (Edinburgh Instruments, FLS920) equipped with an integrating sphere (Jobin-Yvon) and a liquid nitrogen cooled NIR photomultiplier tube (Hamamatsu, R-5587). The samples were mounted at the focal point of the excitation light. For investigating 100% phosphor sample, 5 mm diameter quartz cuvette filled with the powder was used. The error involved in the *UC-QY* measurements is ±10% relative. Absorption spectra of β-$NaYF_4$:Er^{3+} in the PFCB matrix were measured in the integrating sphere of the spectrofluorometer via synchronous scans of the excitation and emission monochromators. Since the $^4I_{11/2} \rightarrow {}^4I_{15/2}$ emission around 980 nm accounts for approximately 97% of the UC emission in β-$NaYF_4$:Er^{3+}, only this transition was considered for the *UC-QY* measurements. To eliminate any contributions of the host lattice and the polymer matrix to the scatter and emission spectra, reference samples with undoped β-$NaYF_4$ powder made with the same concentrations and under the same conditions as the corresponding Er^{3+} doped samples were used. To determine the dependence of the *UC-QY* on the pump power, *QY* and power density were recorded using various ND filters in the excitation beam. The excitation slit width was used to define the area and was kept constant at 20 nm. This ensured that the beam area (square) is same for all the measurements. The beam size was measured using an IR imaging camera (Electrophysics MicronViewer 7290A) and a beam diagnostic software. A total of 238 camera shots were taken and the average beam size was determined as 10.5×10^{-4} cm^2 with a relative error of 0.03%. The beam power was measured by a calibrated germanium photodiode (Newport 818-IR) positioned at the focus of the excitation spot with a 1 μm resolution XYZ stage. The calibration error of the photodiode detector is ±3%. The combined error of calibration (of the photodetector) and uncertainty associated with the power density (in measured power meter readings and the measured area) measurement is ±4.4%. Lifetimes in the IR range were measured with an optical parametric oscillator (OPO) system (Opotek HE 355 II) pumped by the third harmonic of a Nd:YAG laser. This OPO system offers a continuous tunable optical range from 410 to 2400 nm with a pulse width of 10 ns and a repetition rate of 20 Hz. The temporal evolution of the Er^{3+} $^4I_{11/2}$ UC emission at 980 nm at room temperature (RT) upon pulsed $^4I_{13/2}$ excitation at 1523 nm was recorded with a Tektronix 2440 oscilloscope.

III. RESULTS AND DISCUSSION

A. Optimizing the Er^{3+} doping for β-$NaYF_4$: Er^{3+} in a PFCB matrix

In order to optimize the IR→NIR *UC-QY* of β-$NaYF_4$:Er^{3+} in a PFCB matrix, first, the effect of the Er^{3+} doping was investigated. Figure 2(a) shows the $^4I_{15/2} \rightarrow {}^4I_{13/2}$ absorption spectra of pellets with 55.6 w/w% β-$NaYF_4$:Er^{3+}

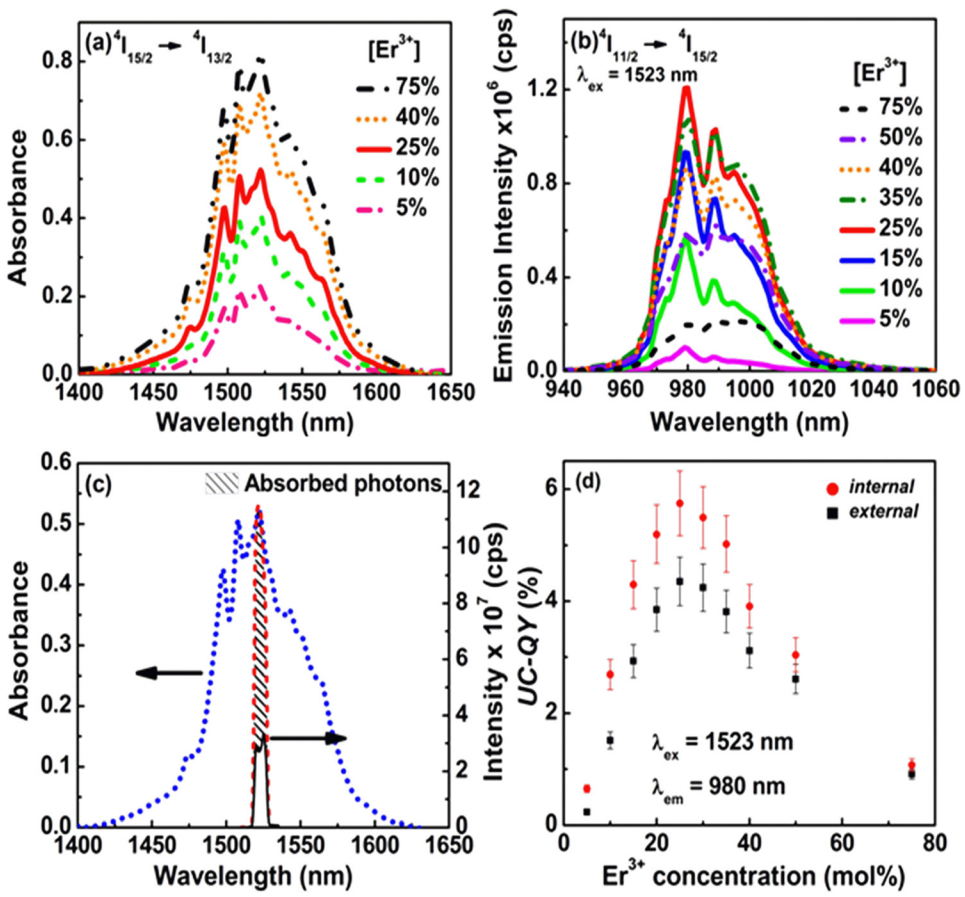

FIG. 2. (a) $^4I_{15/2} \rightarrow {}^4I_{13/2}$ absorption of PFCB pellets with 55.6 w/w% β-$NaYF_4$:Er^{3+} for different Er^{3+} concentrations. (b) $^4I_{11/2} \rightarrow {}^4I_{15/2}$ Er^{3+} emissions for an excitation at 1523 nm with power density of 970 ± 43 Wm^{-2}. (c) Scatter spectra of 25 mol% Er^{3+} sample (black solid curve) and of the corresponding reference sample (red dashed curve). The area under the red dashed curve gives the number of photons incident whereas the difference in the area under the two curves gives the number of photons absorbed. For comparison, the corresponding absorbance spectrum of the sample is shown (blue dotted curve). (d) The *iUC-QY* and *eUC-QY* for different Er^{3+} concentrations of 55.6 w/w% β-$NaYF_4$:Er^{3+} samples in a PFCB matrix at an incident pump power density of 970 ± 43 Wm^{-2}.

in PFCB for different Er^{3+} concentrations. For clarity, only selected spectra out of the whole concentration series are shown. The absorption increases with Er^{3+} doping, but the growth is non-linear for samples with more than 10% Er^{3+}. This effect is attributed to light scattering at phase boundaries, i.e., the samples are not transparent to the excitation light. UC emission spectra were measured for different Er^{3+} concentrations upon monochromatic excitation into the maximum of the $^4I_{13/2}$ excitation band at 1523 nm. Figure 2(b) shows the $^4I_{11/2} \rightarrow {}^4I_{15/2}$ Er^{3+} emission with a maximum at 980 nm for an excitation power density of $970 \pm 43\ Wm^{-2}$. The upconversion emission reaches a maximum at 25 mol% and decreases towards higher doping. In addition, the shape of the emission band changes; and above 25 mol%, a significant increase in intensity of the peaks at 988 nm and 995 nm together with a decrease of the 980 nm peak is observed. Since β-$NaYF_4$:Er^{3+} also absorbs near 980 nm, the observed emission broadening and shift in the maximum emission with increase in Er^{3+} concentration could be related to the radiative trapping. The radiative trapping always occurs in a typical 3-level system when the absorption and emission spectra overlap. Similar emission line broadening effects have been reported in Nd^{3+} doped phosphate glasses, Er^{3+} doped tellurite based glasses, and Er^{3+} doped ultraphosphate glasses.[27] The strength of radiation trapping can be scaled as f_{trap}, i.e., the fraction of emitted radiation which is reabsorbed within the sample, and it can be expressed as $f_{trap} = \Omega\ [1 - \exp(-N_{Er}\ \sigma_a\ V^{1/3})]$, where Ω is the spectral overlap of the emission and absorption bands, N_{Er} Er^{3+} concentration, σ_a the absorption coefficient, and V the sample volume.[27] The larger the value of f_{trap}, the stronger the radiation trapping in the sample. With the increasing of Er^{3+} doping concentration, the fraction of trapped radiation increases, so the 980 nm emission spectrum of Er^{3+} ions broadens accordingly due to the enhanced radiation trapping effect. Figure 2(c) shows the scatter spectra of a 25 mol% Er^{3+} sample (black solid curve) and the undoped reference sample (red dash curve). The area under the red curve gives the number of photons incident, whereas the difference in the area under the two curves gives the number of photons absorbed. For comparison, the corresponding absorbance spectrum of the sample is shown (blue curve). Clearly, even though the β-$NaYF_4$:Er^{3+} sample absorbs in a broad spectral range [between 1480–1580 nm as revealed by the absorbance spectrum], in the present study, only the photons in the bandwidth of 8 nm around excitation wavelength of 1523 nm have been utilized due to monochromatic nature of excitation. The *iUC-QY* and *eUC-QY* for the samples [with 55.6 w/w% of β-$NaYF_4$:Er^{3+} in PFCB matrix] at an incident pump power density of $970 \pm 43\ Wm^{-2}$ are shown in Figure 2(d). The 25 mol% Er^{3+} sample exhibits the highest IR → NIR *iUC-QY* of $5.7\% \pm 0.6\%$ and a corresponding *eUC-QY* of $4.4\% \pm 0.4\%$. Normalization with the power density gives values of $0.59 \pm 0.08\ cm^2\ W^{-1}$ and $0.45 \pm 0.06\ cm^2\ W^{-1}$, respectively. This is a reporting method suggested by Auzel to account for higher efficiencies at higher incident powers, but is limited by saturation of *UC-QY* at higher powers.[10] It is worth to point out that the *UC-QY* at an Er^{3+} concentration of 25 mol% is larger than at 20 mol%, which is the one most commonly used for Si based photovoltaics. The *UC-QY* values for β-$NaYF_4$:20% Er^{3+}, as measured in the present study are $5.2\% \pm 0.5\%$ (internal) and $3.8\% \pm 0.4\%$ (external) implying normalized values of $0.54 \pm 0.08\ cm^2\ W^{-1}$ and $0.39 \pm 0.05\ cm^2\ W^{-1}$, respectively.

The fact that the *UC-QY* increases with the concentration of Er^{3+} up to 25 mol% clearly indicates that the process of energy transfer between the spatially separated Er^{3+} ions rather than the process of excited state absorption involving a single ion dominates the UC mechanism. The *UC-QY* increases with the Er^{3+}concentration due to the combination of a higher absorption and an enhanced probability for energy transfer between the Er^{3+} ions. For Er^{3+} concentrations higher than 25 mol%, the increased delocalization of the excitation results in concentration quenching and reduces the UC emission.[28] These competing effects result in an optimum doping of 25 mol% Er^{3+} for β-$NaYF_4$:Er^{3+}. The optimum concentration reported for NIR to visible emission for Er^{3+} ions in $BaCl_2$ is 28 mol%, whereas that in CaF_2 is approximately 10 mol%, indicating the dependence of the optimum Er^{3+} concentration on host lattice as well. The excitation power densities used in these studies were of the order of $10^4\ Wm^{-2}$.[29,30]

B. Dependence of the *UC-QY* on the excitation power

A two-photon UC process can be identified by a quadratic dependence of the number of UC photons on the excitation power. This is generally true for low excitation power as long as no saturation effects occur.[31] As the UC emission intensity has a quadratic power law dependence on the excitation intensity, the *UC-QY* would therefore have a linear dependence in a log-log plot.[20] To measure the dependence of the *UC-QY* on the excitation power, the PFCB pellets with β-$NaYF_4$:Er^{3+} having different Er^{3+} doping concentrations were excited at the most efficient wavelength of 1523 nm with different laser power densities from $150 \pm 7\ Wm^{-2}$ to $970 \pm 43\ Wm^{-2}$. The deviation from the expected linear behavior of the UC phenomenon is clearly evident in Figures 3(a) and 3(b), showing an increase respectively in the *iUC-QY* and *eUC-QY* as a function of the power density. It is interesting to note that the 25 mol% Er^{3+} samples shows the highest *UC-QY* for all excitation powers studied. The *eUC-QY* on the other hand shifts to higher Er^{3+} concentrations with decrease in power density (because of higher absorption). The log-log plots in Figures 3(c) and 3(d) show linear fits of the *iUC-QY* and *eUC-QY* versus the power density, respectively. For clarity, only a few representative samples are shown. One can identify two regions with different gradients for most of the Er^{3+} concentrations. Table I summarizes the corresponding gradient values and the relevant low and high power regions for different Er^{3+} concentrations. With increasing Er^{3+} concentration, the deviation from the linear slope increases and the point of inflection shifts towards lower power density. This implies that saturation is reached at lower excitation power density in highly doped samples. Similar saturation effects have been observed in Er^{3+} doped fluorozirconate glasses where a shift

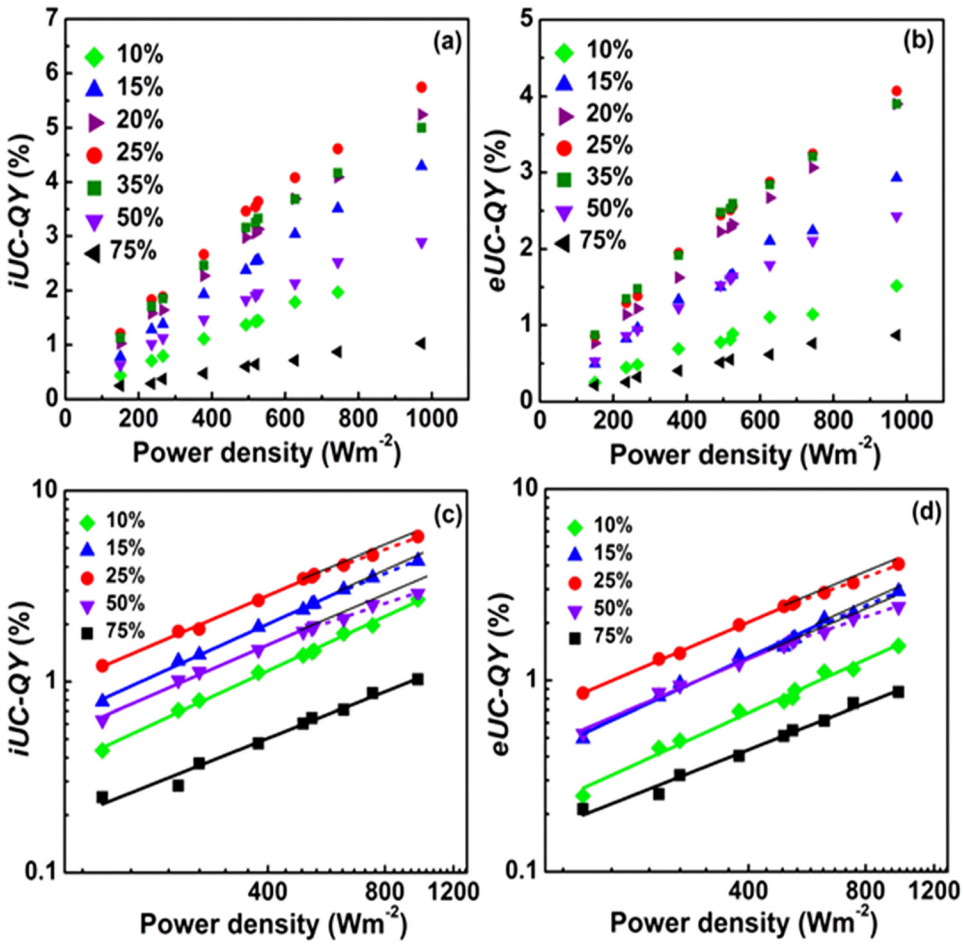

FIG. 3. Variation in the (a) *iUC-QY* and (b) *eUC-QY* as a function of excitation power density for different Er^{3+} concentrations. The log-log plots of the (c) *internal* and (d) *external UC-QY* versus the power density show deviations from a linear behavior for high power density and high Er^{3+} concentrations. The lines are fits to the low (solid lines) and high (dotted lines) power density ranges, respectively. Note that for clarity, the corresponding error values [±10% in the *UC-QY* and ±4.4% in the power density] have not been included in the figures.

in the point of saturation to lower excitation power with increasing Er^{3+} concentration has been observed for NIR to visible *UC-QY*.[32] It may be noted that the reported value of the gradient of log-log plot for the dependence of *eUC-QY* (for IR to visible and NIR upconversion) for β-$NaYF_4$:20%Er^{3+} powder in the low power (<490 Wm^{-2}) region is 0.86 whereas in the higher (440–1050 Wm^{-2}) range is 0.35.[8] The decrease in slope is a well-known behavior in lanthanide doped materials that is related to changes in the rates between the different depopulation mechanisms of the excited states: increased higher order UC processes and cross-relaxations that can, at some point, even compete with the spontaneous radiative emission of the levels.[31] The decreasing slopes are thus due to a saturation of the $^4I_{15/2} \rightarrow {}^4I_{13/2}$ excitation as well as increasing losses by concentration quenching.

TABLE I. (a) The gradient values of linear fits for the log-log plots of the *iUC-QY* versus the power density in the low and high power regions as a function of Er^{3+} doping [in β-$NaYF_4$:Er^{3+} PFCB pellets], see Figure 3(c). (b) The gradient values of linear fits for the log-log plots of the *eUC-QY* versus the power density in the low and high power regions as a function of Er^{3+} doping in β-$NaYF_4$:Er^{3+} PFCB pellets, see Figure 3(d).

	Gradient	
Er^{3+} [mol%]	Low power region	High power region
log-log plots of the *iUC-QY* versus the power density		
10	0.98 (150–970 Wm^{-2})	
15	0.92 (150–625 Wm^{-2})	0.86 (525–970 Wm^{-2})
20	0.87 (150–625 Wm^{-2})	0.82 (525–970 Wm^{-2})
25	0.88 (150–525 Wm^{-2})	0.74 (490–970 Wm^{-2})
35	0.85 (150–490 Wm^{-2})	0.67 (370–970 Wm^{-2})
50	0.84 (150–490 Wm^{-2})	0.68 (370–970 Wm^{-2})
75	0.81 (150–970 Wm^{-2})	
log-log plots of the *eUC-QY* versus the power density		
10	0.94 (150–970 Wm^{-2})	
15	0.93 (150–625 Wm^{-2})	0.87 (525–970 Wm^{-2})
20	0.88 (150–625 Wm^{-2})	0.84 (525–970 Wm^{-2})
25	0.87 (150–525 Wm^{-2})	0.75 (490–970 Wm^{-2})
35	0.86 (150–490 Wm^{-2})	0.66 (490–970 Wm^{-2})
50	0.87 (150–490 Wm^{-2})	0.68 (490–970 Wm^{-2})
75	0.80 (150–970 Wm^{-2})	

C. Mechanism for IR → NIR upconversion in β-$NaYF_4$:Er^{3+}

One of the methods to distinguish an ETU from a GSA/ESA mechanism is by comparing the UC excitation spectrum.[10] Figure 4 illustrates the excitation spectra of the four emission bands: $^4I_{11/2} \rightarrow {}^4I_{15/2}$ at 980 nm, $^4I_{9/2} \rightarrow {}^4I_{15/2}$ at 810 nm, $^4F_{9/2} \rightarrow {}^4I_{15/2}$ at 664 nm, and $^2H_{11/2}$-$^4S_{3/2} \rightarrow {}^4I_{15/2}$ at 542 nm. It is evident that all excitation spectra closely resemble the $^4I_{15/2} \rightarrow {}^4I_{13/2}$ absorption spectrum [blue dotted curve in Figure 2(c)], which clearly indicates the dominance of ETU. The crystal field transition lines show a narrowing with increasing UC exponent of the respective emission. To further investigate the relevant upconversion mechanism involved, the temporal evolution of the Er^{3+} UC emission

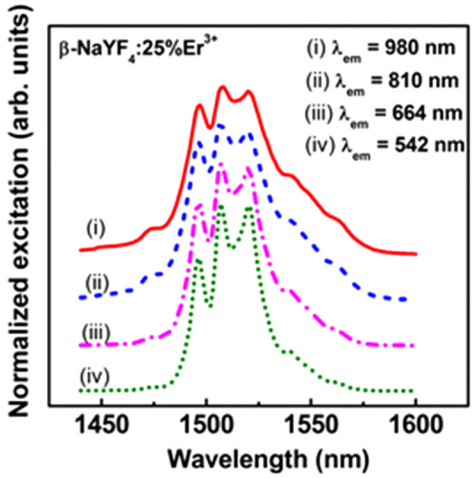

FIG. 4. Normalized excitation spectra of the four Er^{3+} UC emission bands: (i) $^4I_{11/2} \rightarrow {}^4I_{15/2}$ at 980 nm (solid curve), (ii) $^4I_{9/2} \rightarrow {}^4I_{15/2}$ at 810 nm (dashed curve), (iii) $^4F_{9/2} \rightarrow {}^4I_{15/2}$ at 664 nm (dashed-dotted curve), and (iv) $^2H_{11/2}$-$^4S_{3/2} \rightarrow {}^4I_{15/2}$ at 542 nm (dotted curve). All excitation spectra clearly resemble the $^4I_{15/2} \rightarrow {}^4I_{13/2}$ absorption, which indicates that ETU is the dominant UC mechanism.

from the excited state $^4I_{11/2}$ corresponding to the 980 nm emission upon pulsed excitation at 1523 nm into the $^4I_{13/2}$ level is studied at RT. It is known that GSA/ESA is a fast process that usually takes place during the laser pulse (10 ns in our case); and thus, the intensity will show an immediate decay directly after the excitation pulse if GSA/ESA is the dominant mechanism. The GSA/ETU mechanism, on the other hand, requires two ions in their intermediate excited states and a subsequent energy exchange which is a slower process. The energy transfer process populating the emitting state can occur after the laser pulse, therefore a rise in the UC transient after short pulse excitation before exponential decay is observed for ETU process. As the typical time associated with the ETU step is much longer than the 10 ns excitation pulse, the population of the emitting level increases after the short excitation pulse. The UC rise and decay times correlate with the decay rate constants of the intermediate state, the upper excited state, and the energy transfer rate constant.[33] Figure 5(a) shows the RT temporal evolution of the $^4I_{11/2} \rightarrow {}^4I_{15/2}$ Er^{3+} UC emission at 980 nm upon pulsed $^4I_{15/2} \rightarrow {}^4I_{13/2}$ excitation at 1523 nm for samples with 25 and 75 mol% Er^{3+}. The inset in Figure 5(a) shows a semi-log plot for the 25 mol% Er^{3+} sample. The temporal evolution of the 980 nm emission clearly shows a rise and a decay of the luminescence intensity evidencing the ETU processes as the dominant upconversion mechanism. The temporal evolution was fitted to a Vial's type equation,[34] $I(t) = A * \exp(-t/\tau_D) - B * \exp(-t/\tau_R)$, where τ_R and τ_D represent the rise and decay times, respectively. Figure 5(b) shows the rise and decay times for 55.6 w/w% β-$NaYF_4$:Er^{3+} in PFCB pellets as function of the Er^{3+} concentration. The decay and rise times are constant for Er^{3+} concentration up to 25 mol% and decreases for higher Er^{3+} concentrations. This decrease is due to concentration quenching (energy migration to the trap states). Detailed analysis for estimating the life times is out of the scope of this work and would be covered in another publication.

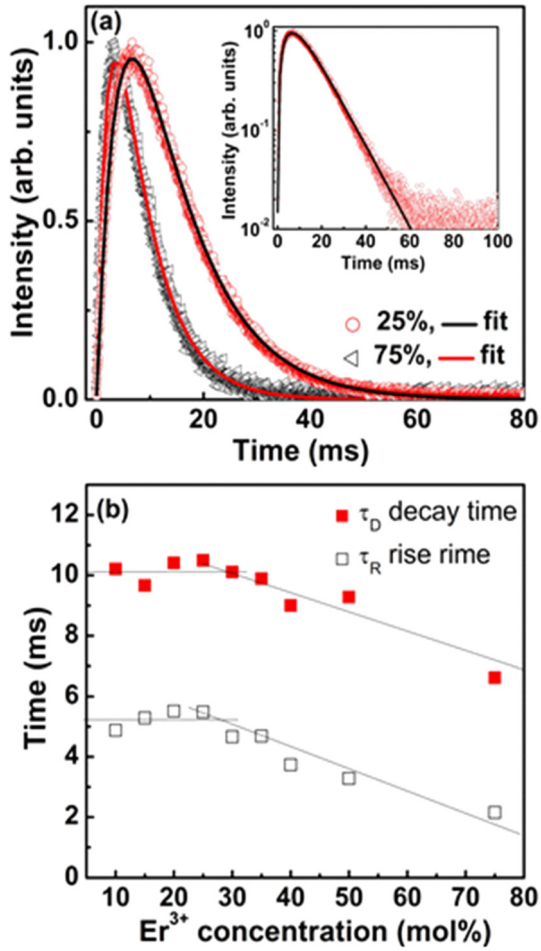

FIG. 5. (a) RT temporal evolution of the $^4I_{11/2}$ UC emission at 980 nm upon pulsed $^4I_{13/2}$ excitation at 1523 nm of β-$NaYF_4$:Er^{3+} samples with 25 mol% and 75 mol% Er^{3+}. The inset shows a semi-log plot for the 25 mol% sample. (b) The rise (open square) and decay (solid square) times for different Er^{3+} concentrations were obtained from fits as shown in (a) to a Vial type equation.[34] The lines are a guide to the eye.

D. Optimizing the β-$NaYF_4$:25%Er^{3+} phosphor concentration in PFCB

In Sec. III A, the maximum *UC-QY* was observed for the sample with 55.6 w/w% $NaYF_4$:25% Er^{3+} in the PFCB pellet. In this section, the phosphor concentration in the PFCB pellets was varied from 55.6 to 84.9 w/w% while the Er^{3+} doping was kept fixed at 25 mol%. Figure 6(a) shows the $^4I_{15/2} \rightarrow {}^4I_{13/2}$ absorption for different amounts of UC phosphor in the PFCB pellets. Figure 6(b) shows the $^4I_{11/2} \rightarrow {}^4I_{15/2}$ UC emission band around 980 nm after excitation at 1523 nm. In contrast to the trend observed with the change in Er^{3+} concentration, as phosphor doping concentration increases, the absorption shows an anomalous behavior. The absorbance increases with the phosphor concentration, reaches a maximum at 75.8 w/w%, and decreases subsequently. The PFCB polymer has an absorption coefficient of 0.3 cm^{-1} at 1523 nm, which implies that with the decrease in polymer concentration, the absorbance of the samples decreases as observed in Fig. 6(a). The UC emission, on the other hand, steadily increases with the phosphor concentration. In contrast to the case of increasing Er^{3+} concentrations [see Figure 2(b)], the band shape of the $^4I_{11/2} \rightarrow {}^4I_{15/2}$ UC emission

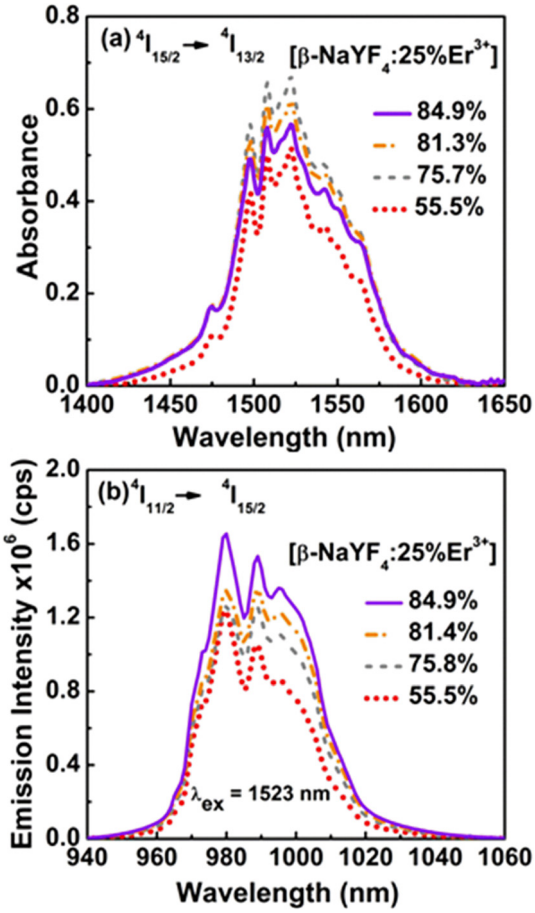

FIG. 6. (a) $^4I_{15/2} \rightarrow {}^4I_{13/2}$ absorption spectra of various concentrations (55.6 to 84.9 w/w%) of β-NaYF$_4$:25%Er^{3+} in PFCB pellets. (b) $^4I_{11/2} \rightarrow {}^4I_{15/2}$ UC emission spectra upon $^4I_{15/2} \rightarrow {}^4I_{13/2}$ excitation at 1523 nm with power density of 970 ± 43 Wm^{-2}.

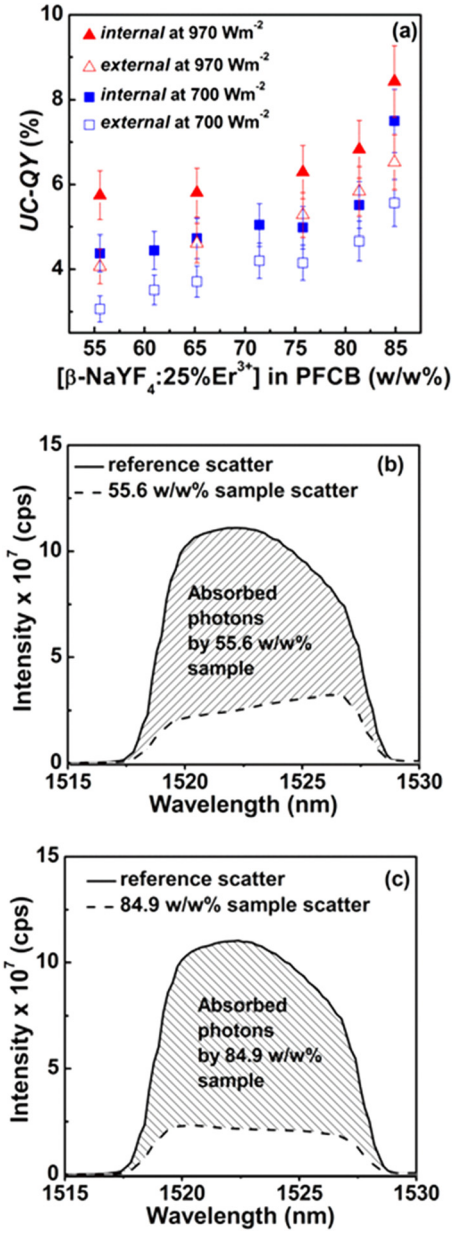

FIG. 7. (a) *Internal* and *external UC-QY* of samples with different concentrations of β-NaYF$_4$:25%Er^{3+} in the PFCB matrix for an incident pump power density of 700 ± 31 Wm^{-2} (up triangles) and 970 ± 43 Wm^{-2} (squares). Scatter spectra of reference (solid curve) and the sample (dashed curve) with (b) 55.6 w/w%, and (c) 84.9 w/w% of β-NaYF$_4$:25%Er^{3+} in PFCB matrix at excitation (1523 nm) power density of 970 ± 43 Wm^{-2}. The difference between the area under the scatter curve for reference and the corresponding sample gives the number of photons absorbed (shaded region). Clearly, the sample with 84.9 w/w% absorbs more photons than the sample with 55.6 w/w% of β-NaYF$_4$:25%Er^{3+} in PFCB matrix.

changes only slightly for different phosphor concentrations. The *iUC-QY* and *eUC-QY* for samples with different concentrations of β-NaYF$_4$:25%Er^{3+} in a PFCB matrix [at incident pump power densities of 700 ± 31 and 970 ± 43 Wm^{-2}] are shown in Figure 7(a). *UC-QY* increases with the UC-phosphor concentration in the range studied. To understand this behaviour, the number of photons absorbed by the samples with 55.6 w/w% and 84.9w/w% of β-NaYF$_4$:25%Er^{3+} in PFCB matrix under 1523 nm excitation at 970 ± 43 Wm^{-2} are compared in Figures 7(b) and 7(c), respectively. The scatter spectra clearly reveal that the sample with more phosphor absorbs more number of photons as compared to the samples with lower phosphor concentration. However, there are no concentration quenching effects observed with increase in phosphor concentration as observed with the increase in the Er^{3+} concentration, and the UC 980 nm emission increases [as shown in Figure 6(b)] resulting in the observed increase in the *iUC-QY* and *eUC-QY* with the increase in phosphor concentration [as shown in Figure 7(a)]. The absence of concentration quenching effects with the increase in phosphor concentration could be related to the decrease in defects and other quenching centres due to incorporation of the phosphor in the polymer lowering the possibility of trapping of the excitation energy. A maximum *iUC-QY* and *eUC-QY* of 8.4% ± 0.8% and 6.5% ± 0.7% respectively, have been achieved for samples with 84.9 w/w% β-NaYF$_4$:25%Er^{3+} in PFCB and an excitation power density of 970 ± 43 Wm^{-2}. This corresponds to normalized *internal* and *external* efficiencies of 0.86 ± 0.12 cm^2 W^{-1} and 0.67 ± 0.10 cm^2 W^{-1}, respectively. These are the highest values reported for β-NaYF$_4$:Er^{3+} under monochromatic excitation. The consistency of these results is evident from a comparison of the data at 700 ± 31 and 970 ± 43 Wm^{-2}.

For comparison, the *iUC-QY* and *eUC-QY* values have been measured for 100% β-NaYF$_4$:25% Er^{3+} powder. An *iUC-QY* and *eUC-QY* of 8.9% ± 0.9% and 4.3% ± 0.4%,

respectively, have been achieved for an excitation power density of $700 \pm 31\ \mathrm{Wm}^{-2}$. Interestingly, whereas the *iUC-QY* of β-$NaYF_4$:25% Er^{3+} powder sample is higher than the sample with 84.9w/w% of β-$NaYF_4$: 25% Er^{3+} in PFCB, the corresponding *eUC-QY* is lower. To understand the observed behaviour, the number of photons absorbed and emitted by the β-$NaYF_4$:25% Er^{3+} powder and the sample with 84.9w/w% of β-$NaYF_4$: 25% Er^{3+} in PFCB (for an excitation of 1523 nm and power density of $700 \pm 31\ \mathrm{Wm}^{-2}$) have been compared in Figures 8(a)–8(c). The number of absorbed photons [difference between the area under the reference scatter and the sample scatter—shaded region as shown in Figures 8(a) and 8(b)] and hence the number of 980 nm UC photons emitted [as shown in Figure 8(c)] by the sample with 84.9w/w% of β-$NaYF_4$: 25% Er^{3+} in PFCB is greater than that by the 100w/w% β-$NaYF_4$:25% Er^{3+} powder. In addition, due to scattering, number of incident photons is less in the powder sample as compared to the 84.9w/w% sample. Also, the trapping of excitation energy in defects and other quenching centres in the powder sample cannot be ruled out. These factors might play a role in the observed lower *eUC-QY* in the powder samples.

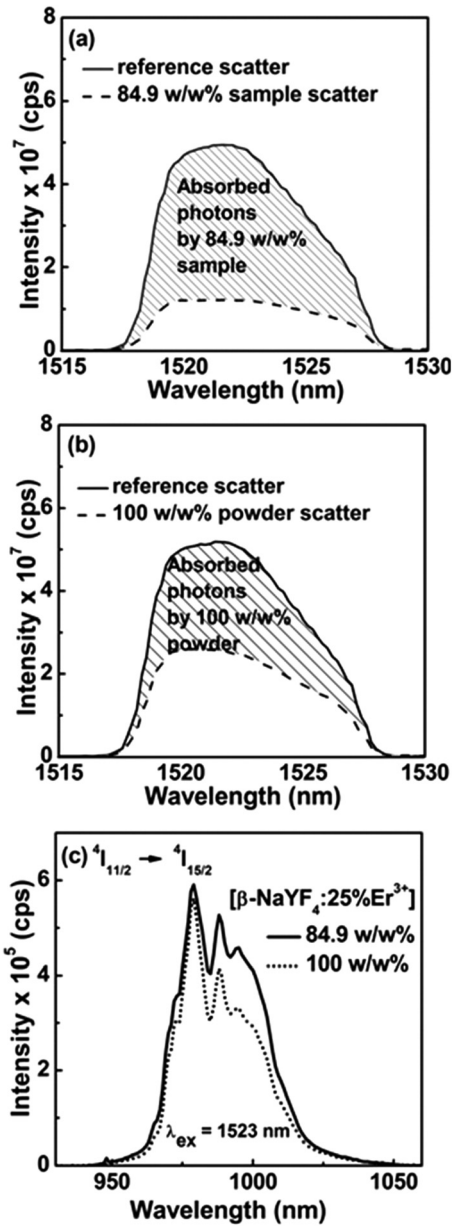

FIG. 8. Scatter spectra of reference (solid curve) and the sample (dashed curve) with (a) 84.9 w/w% of β-$NaYF_4$:25%Er^{3+} in PFCB matrix and (b) 100w/w% β-$NaYF_4$:25%Er^{3+} powder at excitation (1523 nm) power density of $700 \pm 31\ \mathrm{Wm}^{-2}$. The difference between the area under the scatter curve for reference and the corresponding sample gives the number of photons absorbed (shaded region). Clearly, the sample with 84.9 w/w% of β-$NaYF_4$:25%Er^{3+} in PFCB matrix absorbs more photons than the powder sample with 100 w/w% of β-$NaYF_4$:25%Er^{3+}. (c) $^4I_{11/2} \rightarrow {}^4I_{15/2}$ UC emission spectra upon $^4I_{15/2} \rightarrow {}^4I_{13/2}$ excitation at 1523 nm with power density of $700 \pm 31\ \mathrm{Wm}^{-2}$ for 84.9 w/w% (solid curve) of β-$NaYF_4$:25%Er^{3+} in PFCB matrix and 100 w/w% β-$NaYF_4$:25%Er^{3+} powder (dotted curve).

An *eUC-QY* of 3.0% (for IR to visible and NIR) for $880\ \mathrm{Wm}^{-2}$ excitation power was reported for a powder sample of β-$NaYF_4$:Er^{3+} with unoptimized Er^{3+} concentration of 20% [which corresponds to a normalized *external* efficiency of 0.34 $\mathrm{cm}^2\ \mathrm{W}^{-1}$].[8] And the highest *eUC-QY* (for IR to visible and NIR upconversion) of 5.1% is reported for β-$NaYF_4$:20% Er^{3+} powder sample at monochromatic irradiance of $1880\ \mathrm{Wm}^{-2}$ (which corresponds to a normalized *external* efficiency of 0.27 $\mathrm{cm}^2\mathrm{W}^{-1}$).[8] In the present study, on the other hand, the *eUC-QY* (for IR to NIR) of $3.1\% \pm 0.3\%$ and $5.1\% \pm 0.5\%$ for the PFCB pellets with 55.6 w/w% and 84.9 w/w%, respectively, of β-$NaYF_4$: 25% Er^{3+} has been obtained at much lower power density of $700 \pm 31\ \mathrm{Wm}^{-2}$ (which corresponds to a normalized *external* efficiency of $0.44 \pm 0.06\ \mathrm{cm}^2\mathrm{W}^{-1}$ and $0.73 \pm 0.10\ \mathrm{cm}^2\mathrm{W}^{-1}$, respectively).

Higher *iUC-QY* values of 11.5% and 16.7%, respectively, have been reported for IR→NIR upconversion in Er^{3+} doped fluorozirconate glass (ZBLAN) and disordered crystals of YF_3-CaF_2, but at a much higher monochromatic excitation power density of $\sim 10^6\ \mathrm{Wm}^{-2}$.[7] Recently, an IR→NIR *iUC-QY* of 16.2% for PFCB with 55.6 w/w% β-$NaYF_4$:10% Er^{3+} has been demonstrated for a sample that had neither been optimized in Er^{3+} concentration nor the phosphor concentration, using a broadband excitation (bandwidth of 61 nm) and a power density of $\sim 2 \times 10^6\ \mathrm{Wm}^{-2}$.[21] Both of these power density values are much higher than those used for PV applications. However, using the optimized Er^{3+} dopant and phosphor concentration and an ideal matrix in conjunction with broadband excitation and emerging technologies (such as spectral concentration using quantum dots,[35] or photonic structures,[36] or near field enhancement using plasmonic structures[37,38]) would significantly improve efficiencies of low-power solar upconversion. This would make achieving a single-junction solar cell with efficiency beyond the Shockley–Queisser limit a reality.

IV. CONCLUSIONS

The present study reports for the first time the optimization of the IR (1523 nm) → NIR (980 nm) upconversion of β-$NaYF_4$:Er^{3+} embedded in a PFCB matrix under monochromatic excitation. For an optimum Er^{3+} doping of 25 mol% and a phosphor concentration of 84.9 w/w% an *iUC-QY* of $8.4\% \pm 0.8\%$ (and *eUC-QY* of $6.5\% \pm 0.7\%$) has been achieved for 1523 nm excitation at $970 \pm 43\ \mathrm{Wm}^{-2}$. This corresponds to normalized *internal* and *external* efficiencies of

$0.86 \pm 0.12\,cm^2\,W^{-1}$ and $0.67 \pm 0.10\,cm^2\,W^{-1}$, respectively. This is the highest reported *UC-QY* for β-$NaYF_4$:Er^{3+} under monochromatic excitation. The special characteristics of both the UC phosphor β-$NaYF_4$:Er^{3+} and the PFCB matrix give rise to this outstanding *UC-QY*. β-$NaYF_4$ is a low phonon host material with maximum phonon energy of about $350\,cm^{-1}$. It has no multi-phonon relaxation losses from the $^4I_{13/2}$ and $^4I_{11/2}$ states. Also the $^4I_{15/2} \rightarrow {}^4I_{13/2}$ absorption is reasonably strong for an efficient excitation. The Er^{3+} sites with microscopic disorder make β-$NaYF_4$:Er^{3+} one of the best UC phosphors. The PFCB matrix has a low absorbance in the relevant IR and NIR spectral regions. Due to fluorination, high frequency C-H or O-H acceptor vibrations are absent in this matrix. Additionally, PFBC matches the refractive index of the UC phosphor quite closely. The time dependent measurements reveal that the UC processes in β-$NaYF_4$:Er^{3+} proceed via ETU.

ACKNOWLEDGMENTS

The authors gratefully acknowledge the funding from the European Community's Seventh Framework Program (FP7/2007-2013) under Grant Agreement No. 246200 with in the 'Nanospec' project - "Nanomaterials for harvesting sub-band-gap photons via upconversion to increase solar cell efficiencies".

[1]See http://www.ise.fraunhofer.de/de/downloads/pdf-files/aktuelles/photovoltaics-report.pdf for up-to-date information (till Dec 2012) about the PV market, efficiencies of solar cells and modules, price development and Energy payback time.
[2]W. Shockley and H. J. Queisser, J. Appl. Phys. **32**, 510 (1961).
[3]T. Trupke, M. A. Green, and P. Würfel, J. Appl. Phys. **92**, 4117 (2002); A. C. Atre and J. A. Dionne, *ibid.* **110**, 034505 (2011); C. M. Johnson and G. J. Conibeer, *ibid.* **112**, 103108 (2012).
[4]A. Shalav, B. S. Richards, T. Trupke, K. W. Krämer, and H. U. Güdel, Appl. Phys. Lett. **86**, 013505 (2005); A. Shalav, B. S. Richards, and M. A. Green, Sol. Energy Mater. Sol. Cells **91**, 829 (2007); B. S. Richards and A. Shalav, IEEE Trans. Electron Devices **54**, 2679 (2007).
[5]C. Strümpel, M. McCann, G. Beaucarne, V. Arkhipov, A. Slaoui, V. Švrček, C. D. Cañizo, and I. Tobias, Sol. Energy Mater. Sol. Cells **91**, 238 (2007).
[6]A. C. Pan, C. del Cañizo, and A. Luque, Mater. Sci. Eng. B **159–160**, 212 (2009).
[7]S. Ivanova and F. Pellé, J. Opt. Soc. Am. B **26**, 1930 (2009); F. Pellé, S. Ivanova and J.-F. Guillemoles, EPJ Photovolt. **2**, 20601 (2011).
[8]S. Fischer, J. C. Goldschmidt, P. Löper, G. H. Bauer, R. Bruggemann, K. Krämer, D. Biner, M. Hermle, and S. W. Glunz, J. Appl. Phys. **108**, 044912 (2010).
[9]J. de Wild, J. K. Rath, A. Meijerink, W. G. J. H. M. van Sark, and R. E. I. Schropp, Sol. Energy Mater. Sol. Cells **94**, 2395 (2010).
[10]F. Auzel, Chem Rev. **104**, 139 (2004).
[11]F. Auzel, F.C.R. Acad. Sci (Paris) **262**, 1016 (1966); **263**, 819 (1966); V. Ovsyankin and P. P. Feofilov, JETP Lett. **3**, 317 (1966); **3**, 322 (1966).
[12]M. Mohageg, A. B. Matsko, and L. Maleki, Opt. Express **20**, 16704 (2012).
[13]D. V. Seletskiy, S. D. Melgaard, S. Bigotta, A. D. Lieto, M. Tonelli, and M. Sheik-Bahae, Nature Photon. **4**, 161 (2010).
[14]M. Quintanilla, E. Cantelar, F. Cussó, M. Villegas, and A. C. Caballero, Appl. Phys. Express **4**, 022601 (2011); B. Dong, B. Cao, Y. He, Z. Liu, Z. Li, and Z. Feng, Adv. Mater. **24**, 1987 (2012).
[15]Z. Li, Y. Zhang, and S. Jiang, Adv. Mater. **20**, 4765 (2008).
[16]N. M. Idris, M. K. Gnanasammandhan, J. Zhang, P. C. Ho, R. Mahendran, and Y. Zhang, Nat. Med. **18**, 1580 (2012).
[17]F. Wang, Y. Han, C. S. Lim, Y. Lu, J. Wang, J. Xu, H. Chen, C. Zhang, M. Hong, and X. Liu, Nature **463**, 1061 (2010).
[18]G. H. Dieke and H. M. Crosswhite, Appl. Opt. **2**, 675 (1963).
[19]A. Aebischer, M. Hostettler, J. Hauser, K. Krämer, T. Weber, H. U. Güdel, and H. B. Bürgi, Angew. Chem. **118**, 2869 (2006).
[20]C. Renero-Lecuna, R. Martín-Rodríguez, R. Valiente, J. González, F. Rodríguez, K. W. Krämer, and H. U. Güdel, Chem. Mater. **23**, 3442 (2011).
[21]S. K. W. MacDougall, A. Ivaturi, J. Marques-Hueso, K. W. Krämer, and B. S. Richards, Opt. Express **20**, A879 (2012).
[22]Y. K. Olsson, G. Chen, R. Rapaport, D. T. Fuchs, V. C. Sundar, J. S. Steckel, M. G. Bawendi, A. Aharoni, and U. Banin, Appl. Phys. Lett. **85**, 4469 (2004).
[23]R. E. Thoma, H. Insley, and G. M. Hebert, Inorg. Chem. **5**, 1222 (1966).
[24]J. Gordon, J. Ballato, D. W. Smith, Jr., and J. Jin, J. Opt. Soc. Am. B **22**, 1654 (2005).
[25]D. W. Smith, Jr., S. Chen, S. M. Kumar, J. Ballato, C. Topping, H. V. Shah, and S. H. Foulger, Adv. Mater. **14**, 1585 (2002).
[26]K. W. Krämer, D. Biner, G. Frei, H. U. Güdel, M. P. Hehlen, and S. R. Lüthi, Chem. Mater. **16**, 1244 (2004).
[27]P. R. Ehrmann and J. H. Campbell, J. Am. Ceram. Soc. **85**, 1061 (2002); X. Feng, S. Tanabe, and T. Hanada, J. Appl. Phys. **89**, 3560 (2001); Z. Y. Xun, X. X. Chen, C. Fen, L. J. Hui, and Y. G. Bo, Opt. Electron. Lett. **8**, 0273 (2012).
[28]D. L. Dexter and J. H. Schulman, J. Chem. Phys. **22**, 1063 (1954).
[29]J. Ohwaki and Y. Wang, Electon. Lett. **29**, 351 (1993).
[30]S. Pollack, D. Chang, and N. Moise, J. Appl. Phys. **60**, 4077 (1986).
[31]M. Pollnau, D. Gamelin, S. Luthi, H. U. Güdel, and M. P. Hehlen, Phys. Rev. B **61**, 3337 (2000).
[32]B. Henke, F. Pientka, J. A. Johnson, B. Ahrens, P. T. Miclea, and S. Schweizer, J. Phys.: Condens. Matter **22**, 155107 (2010).
[33]D. R. Gamelin and H. U. Güdel, *in Transition Metal and Rare Earth Compounds—Excited States, Transitions, Interactions II*, Topics in Current Chemistry Vol. 214, edited by H. Yersin (Springer-Verlag, Berlin, 2001), pp 1–56.
[34]R. Buisson and J. C. Vial, J. Phys. (France) Lett. **42**, 115 (1981).
[35]A. C. Pan, C. del Cañizo, E. Cánovas, N. M. Santos, J. P. Leitão, and A. Luque, Sol. Energy Mater. Sol. Cells **94**, 1923 (2010).
[36]C. M. Johnson, P. J. Reece, and G. J. Conibeer, Opt. Lett. **36**, 3990 (2011).
[37]A. C. Atre, A. García-Etxarri, H. Alaeian, and J. A. Dionne, J. Opt. **14**, 024008 (2012).
[38]W. Zhang, F. Ding, and S. Y. Chou, Adv. Mater. **24**, OP236 (2012).